Shear-slip behaviour of prefabricated composite shear stud connectors in composite bridges

Gao, Yanmei; Li, Chengjun; Wang, Xuefei; Zhou, Zhixiang; Fan, Liang; Heng, Junlin

DOI
10.1016/j.engstruct.2021.112148

Publication date
2021

Document Version
Accepted author manuscript

Published in
Engineering Structures

Citation (APA)
Gao, Y., Li, C., Wang, X., Zhou, Z., Fan, L., & Heng, J. (2021). Shear-slip behaviour of prefabricated composite shear stud connectors in composite bridges. *Engineering Structures*, *240*, 1-16. Article 112148. https://doi.org/10.1016/j.engstruct.2021.112148

Shear-Slip Behaviour of Prefabricated Composite Shear Stud Connectors in Composite Bridges

Yanmei Gao[1], Chengjun Li[2], Dong Liu[1], Zhixiang Zhou[3], Liang Fan[1], Junlin Heng[3,4]

[1] Department of Bridge Engineering, School of Civil Engineering, Chongqing Jiaotong University, Chongqing 400074, China

[2] Department of Road and Bridge Engineering, Sichuan Vocational and Technical College of Communications, Chengdu 611130, China

[3] Department of Civil Engineering, College of Civil and Transportation Engineering, Shenzhen University, Shenzhen 518060, China

[4] Department of Engineering Structures, School of Civil Engineering and Geosciences, Delft University of Technology, Delft 2628 CN, The Netherlands

Abstract: This paper has investigated the shear-slip behaviour of an innovative prefabricated composite shear stud (PCSS) connector and its application in the prefabricated steel-concrete composite bridges. A series of push-out tests are carried out on a total of 12 specimens, including 6 PCSS specimens and 6 conventional shear stud (CSS) specimens. Further comparison has been carried out between the test result and the data available from the literature. Based on the test, a high-resolution finite element (FE) analysis has been performed to reveal the load transfer mechanism of the PCSS connector at the component-level. After that, an advanced FE model has been established and validated by a full-scale test of the prefabricated composite bridge using the PCSS. With the FE model, the load-slip behaviour and slip distribution are investigated in details. The result highlights the enhanced shear capacity and ductility of the PCSS specimens compared with the CSS specimens, as well as the feasibility of PCSS connectors in composite bridges. Meanwhile, it is further revealed by the detailed investigation that the enhancement could be attributed to the lateral constraint on the concrete by the vertical steel plate in the PCSS. Besides, it is also found that the load-slip behaviour of composite bridges using the PCSS is influenced by the cracking at the seam between deck blocks. Consequently, abrupt changes can be found in the load-slip curve once the cracking occurs, which differs from the traditional composite bridges.

Keywords: prefabricated composite shear studs connector; prefabricated steel-concrete composite bridge; push-out test; high-resolution finite element analysis; shear-slip behaviour; load-transfer mechanism.

1. Introduction

Steel-concrete composite bridges are extensively applied worldwide since they efficiently utilise mechanical features of both the steel and concrete materials. The concrete bridge deck is usually connected to the steel structures through shear connectors, by which the two members can work together compatibly [1]. Apart from the advantages, several challenges remain in the application of accelerated bridge construction (ABC) in composite bridges, especially in connecting the steel and concrete during the in-site erection. Thus, extra efforts are required to build the composite bridge in the ABC way [2]. On this end, the pre-cast decks and in-site connections are gradually employed in composite bridges, which can notably accelerate the construction and minimise the effect of shrinkage and creep in the concrete deck [3]-[8].

Extensive research efforts have been made by researchers worldwide respecting the application of pre-cast concrete decks in composite bridges, and several types of shear connectors were proposed in accordance. As per the configuration and mechanical features, the proposed shear connectors can be divided into 4 types, including the clustered shear stud connector, distributed shear stud connector, and embossed steel plate connector and friction-based shear connector, as shown in Figs. 1a to d.

The clustered shear stud connector (shown in Fig. 1a) is currently the most popular type due to its matureness in engineering practices. In the connector, the studs are arranged group-by-group at multiple locations on the top surface of steel members. In the erection, the concrete deck is at first prefabricated in the casting yard with a series of post-cast holes reserved. After that, the pre-cast deck is installed on the steel girder in the construction field, with the shear studs accommodated within the reserved holes. Then the holes will be filled in with the cast-in-situ concrete to connect the deck and steel girder. To date, considerable research efforts have been made on the clustered shear stud. Through static tests, Shim et al. [9] investigated the influence of key design parameters on the mechanical performance of shear studs. The studied parameters include the spacing between studs, hooping parameter and stud diameter. According to the result, the ultimate strength of the connector decreases with the spacing between studs, which can be considered by a proposed empirical equation. Xiang et al. [10] studied the mechanical behaviour of composite beams with the different layout of studs, using the static test and finite element analysis. The result suggested that no explicit relationship was found between the layout

of the studs and the loading capacity of composite beams. Wang et al. [11] carried out a series of tests to investigate the influence of the shape of the reserved holes, including the rectangular hole and circular hole. The result indicated that the mechanical performance of connectors is better with rectangular holes than with circular holes. Sjaarda et al. [12] conducted the fatigue test of the composite beam with cluster shear studs, indicating that the fatigue performance is compatible with the cast-in-situ deck.

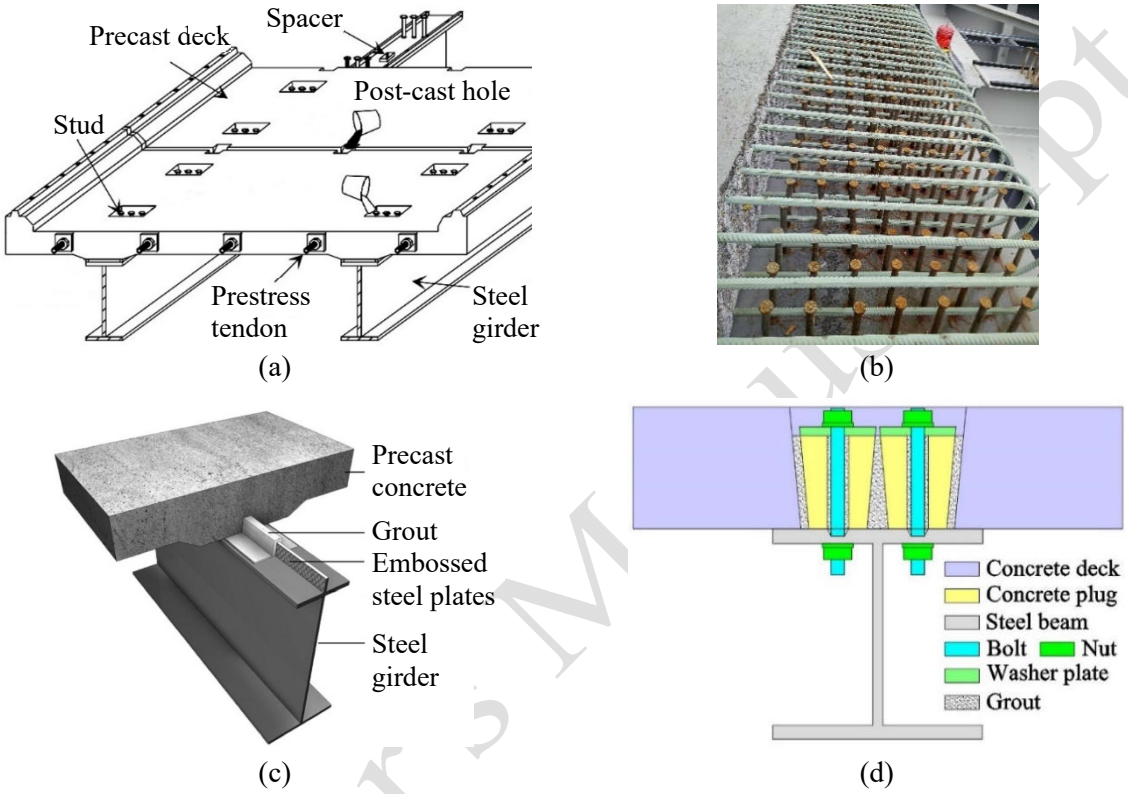

Fig. 1. Four typical types of prefabricated shear connectors: (a) clustered shear stud connector - adapted from [9]; (b) distributed shear stud connector - courtesy of Dr Yanmei GAO; (c) embossed steel plate connector - adapted from [14]; (d) friction-based shear connector – adapted from [16].

The distributed shear stud connector is an alternative solution to the clustered shear stud connector [2]. As shown in Fig. 1b, the studs are uniformly placed along the longitudinal direction of the deck, and the continuous post-cast strip is left to accommodate the studs instead of the hole. Compared with clustered studs, the distribution of shear force becomes more even in distributed studs due to the decentralization. As a result, the concrete deck works with the steel girder in a more compatible way. However, according to Liu et al. [13], the mechanical behaviour of the composite bridge using distributed studs is almost the same as the one using clustered studs. It is worth noting that the distributed shear stud was proposed by FWHA [15] as the standard design for the steel-concrete connection in prefabricated steel-concrete composite bridges.

The embossed steel plate connector [14] is different from the above two connectors using studs. As shown in Fig. 1c, the embossed steel plate is vertically welded to the top surface of the steel beam, which will be accumulated by the reserved post-cast strip when assembling. The post-cast strip is then filled in with the high-grade grout to combine the vertical steel plate with the concrete deck. According to the static and fatigue tests, the mechanical capacity of the embossed steel plate connector is almost the same as that of the shear stud-based connectors.

The layout of the friction-based shear connector (FBSC) [16] is similar to the clustered shear stud connector, as shown in Fig.1d, except that preloaded bolts are used instead of shear studs. As a result, the shear force between the deck and steel member is transferred through the friction force rather than the deformation of studs. As per the push-out tests of 11 specimens, it was claimed that a higher shear capacity could be expected in the FBSC compared with the shear stud connector.

A common feature of the above connectors is that the post-cast hole or strip should be reserved in the pre-cast deck in advance. As per the relevant studies [9], [17], cracks are highly prone to initiate from the corner of these post-cast holes or strips. The cracking can be mainly attributed to the following two factors: (1) high-level stress concentration exists in the corner of the holes or strips due to the age difference between the pre- and post-cast concretes; (2) the prestress applied by tendons cannot be effectively transferred to the shear holes or strips. Meanwhile, cracks are also likely to initiate in the cast-in-situ seam between different segments of the deck, which mainly depends on the quality of the post-cast mortar and the effective prestress.

Recently, several types of post-casting-free shear connectors were proposed for building structures, including the through-bolt connector [18][19] and friction-grip bolt connector [20]. However, these connectors are not feasible with the employment of the prestress, which largely limits their application in composite bridges.

In dealing with the discussed issues, an innovative prefabricated composite shear stud (PCSS) connector has been proposed [21][22]. In the PCSS, no post-cast work is required, and the prestress can be easily applied in the concrete deck in an efficient way. The feasibility of the PCSS connector has been preliminarily verified through the fabrication experiment [23]. However, due to the limited number

of specimens, the shear-slip behaviour, which reflects the load transfer between the concrete and steel, has not yet been illustrated in detail for the composite bridges using the PCSS.

This study aims to investigate the shear-slip behaviour of the PCSS connector and further reveal the mechanism of load transfer between the concrete and steel in composite bridges using the PCSS. In Section 2, a total of 12 push-out specimens have been tested, including 6 PCSS specimens and 6 specimens with conventional shear stud (CSS) connectors. Based on the present test and the data from the literature, further comparison has been made on the shear-slip behaviour between the PCSS and the CSS. Moreover, high-resolution finite element (FE) analysis has been conducted to reveal the mechanical behaviour of the PCSS specimen. In Section 3, further investigation has been carried out on the distribution of the slip and load transfer mechanism in the composite bridge using the PCSS, including both the full-scale model test and refined FE analysis. In Section 4, the major conclusions are drawn from the study. In summary, the outputs can serve as the guideline for the research, design and fabrication of composite bridges using PCSS connectors.

2. Push-out test of PCSS connector

2.1 Innovation of the PCSS connector

The prefabricated composite shear stud (PCSS) connector is proposed to improve the application of ABC in composite bridges, as shown in Fig. 2. The PCSS connector consists of two steel plates, with a series of distributed shear studs welded on. When casting the concrete deck, the two vertical steel plates serve as sheets, with the studs embedded in the concrete. Then the prestress is applied to the deck through tendons after the deck is installed in place.

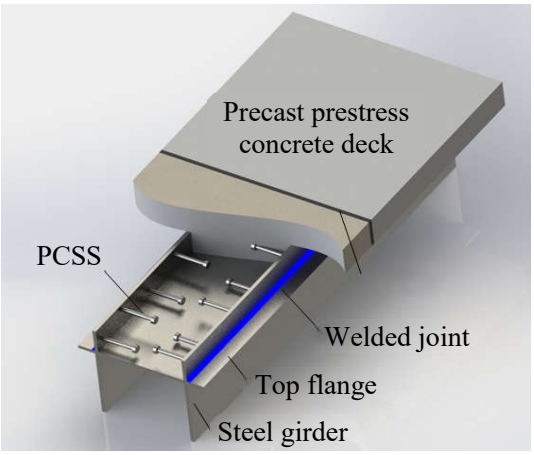

Fig. 2. Design of the prefabricated composite shear stud connector.

It is worth noting that the steel girder and concrete deck are not connected during the pretension, so that the prestress can be effectively transferred to the concrete deck. After that, the two steel plates are welded to the top flange of the steel girder, through which the deck and the steel girder are connected. Apparently, the post-casting hole or strip is no longer required when using the PCSS. As a result, the configuration of the deck is notably simplified as well as the fabrication process. Moreover, the post-cast concrete is replaced by the welded connection, whose quality is easier to control by the application of proper welding technology and quality assurance. As a result, the PCSS is expected to eliminate the cracking issue of the concrete deck induced by the age difference.

2.2 Design of comparative push-out tests

2.2.1 Configuration of specimens

A series of comparative push-out tests are carried out to investigate the shear-slip behaviour of the novel PCSS connector, including a total of 12 specimens. The specimens are respectively fabricated with two types of connectors, i.e., the PCSS and conventional shear stud (CSS). Within each type, the specimens can be classified into two groups by the row of studs, i.e., 3 or 4 rows. Table 1 shows the details about the classification of the specimens.

Table 1 Classification of specimens

Type	Group	Stud layout	Row of studs	Connection	Number of specimens
PCSS	HS3	Horizontal	3	Welding	3
	HS4	Horizontal	4	Welding	3
CSS	VS3	Vertical	3	Casting-in-situ	3
	VS4	Vertical	4	Casting-in-situ	3

It is worth noting that, the PCSS specimens are fabricated with the horizontal stud (HS), while the vertical stud (VS) is employed in the CSS specimens. For better illustration, the specimens are named after the layout and number of studs, followed by the serial number of the specimen within the group. The configuration of the CSS and PCSS specimens are shown in Figs. 3 and 4, respectively. The specimen consists of a hollow steel box in the middle and a T-shaped concrete deck at both sides, connected either by the PCSS or CSS. The steel box is 530 mm long, 150 mm wide and 116 mm deep, with the plate thickness of 8 mm. Meanwhile, the concrete deck is 500 mm long, 300 mm wide and 200 mm deep, with the reinforcement of 8 mm in diameter. In both the type of connections, the size of studs

149 is Φ10 mm×50 mm, i.e., 10 mm in diameter and 50 mm in height. At the top of the stud, a 7 mm-thick
150 cap is designed to prevent the concrete from pulling up, with an enlarged diameter of 18 mm. In the
151 PCSS specimen, the vertical steel plate is 100 mm-high and 8 mm-thick, to which the studs are welded.

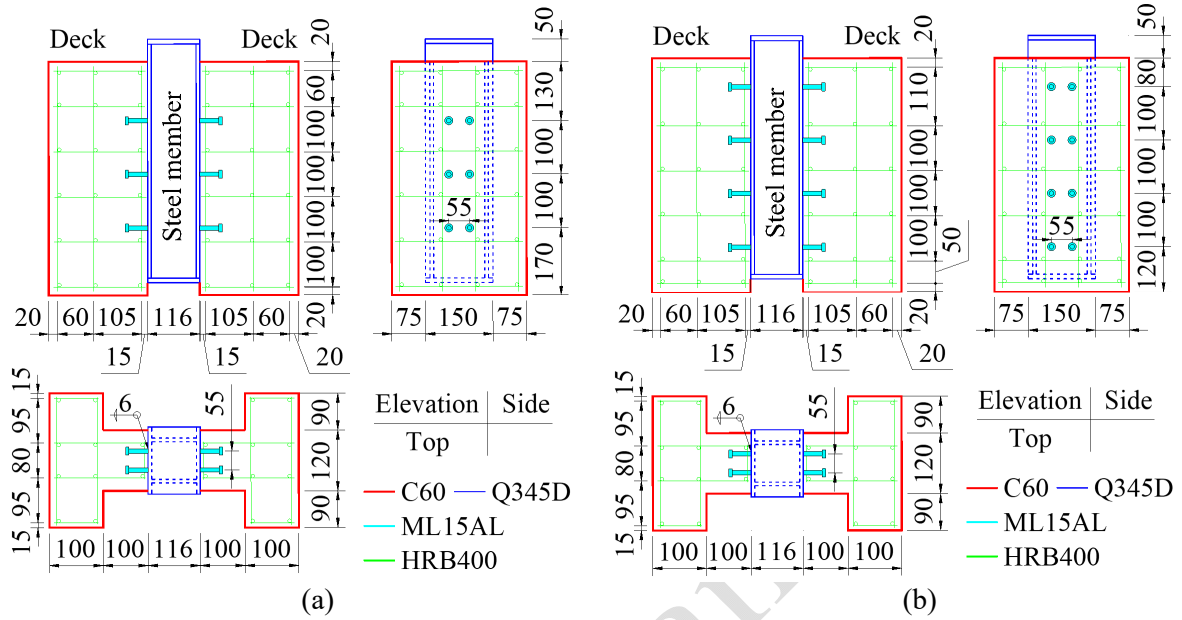

152 **Fig. 3.** Layout of CSS specimen (Unit: mm): (a) VS3; (b)VS4.

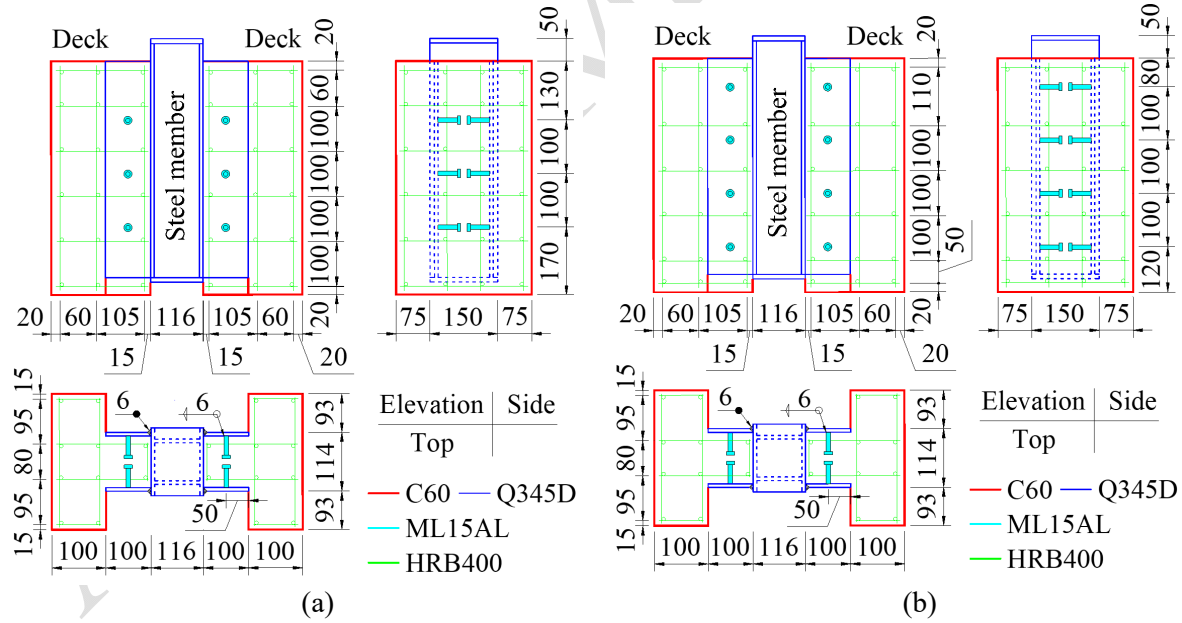

153 **Fig. 4.** Layout of PCSS specimen (Unit: mm): (a) HS3; (b) HS4.

154 Different fabrication procedures are employed for the PCSS and CSS specimens, respectively. In
155 the CSS specimen, the studs are directly welded to the top flange of the steel box and then covered
156 within the concrete deck when casting. In the PCSS specimen, the studs are at first welded to the vertical
157 steel plate. The concrete deck is then cast between vertical plates, with the studs embedded. Finally, the

158 deck is connected to the top flange of the steel box through the fillet welded joint, as shown in Fig. 2.
159 In both types of specimens, continuous fillet welded joints are employed to connect the studs with the
160 steel plate, with a weld leg length of 6 mm. Similarly, the fillet welded joint has also been employed in
161 the vertical plate-to-flange connection in the PCSS specimens, with a length of 6 mm. The welds are
162 performed by flux-cored arc welding (FCAW) protected with CO_2, using the manual welding machine.
163 In the fabrication, the structural steel Q345D [24] is used for the steel member and the vertical
164 plate, while the cold-forging steel M15AL [24] is chosen for the shear studs as per the rule of
165 performance protection. The deck is made of the concrete C60 [25], with the reinforcement of the steel
166 bar HRB400 [25]. Prior to the push-out test, static material tests have been carried out to obtain the
167 basic mechanical properties of the testing materials. The measured material data are shown in Table 2.

168 **Table 2** Measured mechanical properties of the testing materials

Shear stud			Steel box/plate		Reinforcement		Concrete deck	
Elastic modulus (GPa)	Yielding strength (MPa)	Ultimate strength (MPa)	Elastic modulus (GPa)	Yielding strength (MPa)	Elastic modulus (GPa)	Yielding strength (MPa)	Elastic modulus (GPa)	Cubic strength (MPa)
205	340	430	195	365	209	458	34.6	62.1

169 *2.2.2 Test Setup*

170 Static loading tests have been carried on the specimens using a hydraulic testing machine with a
171 maximum capacity of 10,000 kN, as shown in Fig. 5. During the test, electronic dial gauges have been
172 installed between the root of studs and the concrete to measure the relative displacement between the
173 concrete deck and the steel box, i.e., the slip. The installed dial gauges have a maximum range of 10
174 mm and a resolution of 0.001 mm. Before loading, a target force F_t has been calculated using an analytic
175 model proposed to solve the ultimate capacity in [24]. According to the model, the ultimate capacity of
176 the specimen is controlled by the shear fracture of studs. At the same time, the failure of studs will also
177 be influenced by the concrete surround them, as shown in Equation 1.

178
$$N_t^c = \sum_{v=1}^{n_{std}} N_v^c \quad (1a)$$
$$N_v^c = 1.19 A_{std} f_{std} (E_c/E_S)^{0.2} (f_{cube}/f_{std})^{0.1} \quad (1b)$$

179 Where N_t^c and N_v^c are the total capacity and the capacity of single stud; n_{std} is the number of studs;
180 A_{std} stands for the sectional area of studs; E_c and E_s are the elastic modulus of the concrete and stud;
181 f_{cube} and f_{std} are respectively the cubic strength of the concrete and the uniaxial strength of the stud.

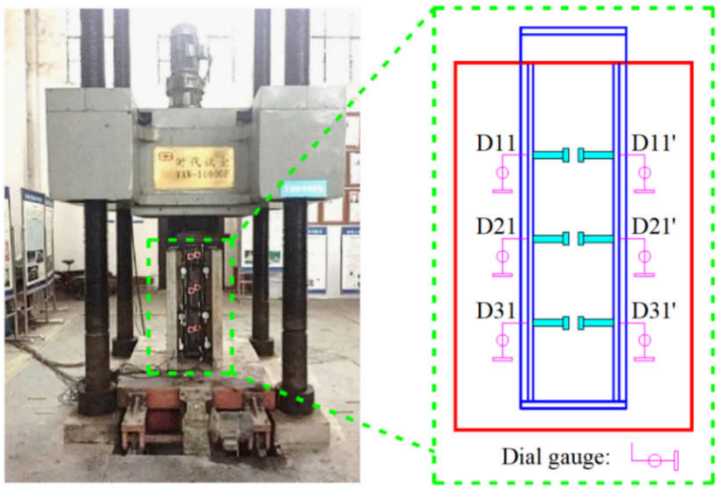

Fig. 5. Set up of the static loading test (HS3-2).

Based on the target force, a total of 5 loading cycles is applied to each specimen, as illustrated in Table 3. In the 1st loading cycle, a preload with 10% of the target force is loaded and unloaded. After that, 3 cycles with 30% of the target force are applied with an increment of 5%. In the final cycle, i.e. the 5th cycle, the specimen is loaded to failure with an increment of 10% of the target force. During the test, the measurement is carried out after each loading step. Besides, it is worth stating that in the 5th cycle, the applied loading force can be increased beyond the target load until the failure of the specimen is achieved.

Table 3 Loading prototypes

Loading cycle	Type	Prototype
1st	Preload	$0 \rightarrow 0.03F_t \rightarrow 0.06F_t \rightarrow 0.1F_t \rightarrow 0.06F_t \rightarrow 0.03F_t \rightarrow 0$
2nd ~ 4th	Cyclic	$0 \rightarrow 0.05F_t \rightarrow 0.1F_t \rightarrow 0.15F_t \rightarrow 0.2F_t \rightarrow 0.25F_t \rightarrow 0.3F_t \rightarrow 0.25F_t \rightarrow 0.2F_t \rightarrow 0.15F_t \rightarrow 0.1F_t \rightarrow 0.05F_t \rightarrow 0$
5th	Ultimate	$0 \rightarrow 0.1F_t \rightarrow 0.2F_t \rightarrow 0.3F_t \rightarrow 0.4F_t \rightarrow 0.5F_t \rightarrow 0.6F_t \rightarrow 0.7F_t \rightarrow 0.8F_t \rightarrow 0.9F_t \rightarrow F_t$

2.3 Test results

2.3.1 Load-slip curve

Based on the measurement, the relation can be established respecting the load and the slip between the concrete deck and steel studs. The measured load-slip curves are illustrated in Figs. 6a to d, in which the average slip from the dial gauges in Fig. 5 is used. Generally, the curves can be divided into two stages, i.e., the ascending and descending stages. The ascending stage can be further classified as the linear and nonlinear parts, which are diverged at roughly 50% of the ultimate load.

Similarly, Oehlers and Bradford suggested the stud remains elastic before 50% of the ultimate load and the modulus could be regarded as a constant value [26]. Within the linear part, the slip increases slowly and proportionally with the applied load, indicating the elastic deformation of the specimen. The slip can be recovered after unloaded within the linear part, further demonstrating the pure elastic behaviour. When the load increases beyond 50% of the ultimate load, nonlinearity can be observed in the load-slip curve, indicating plastic deformation.

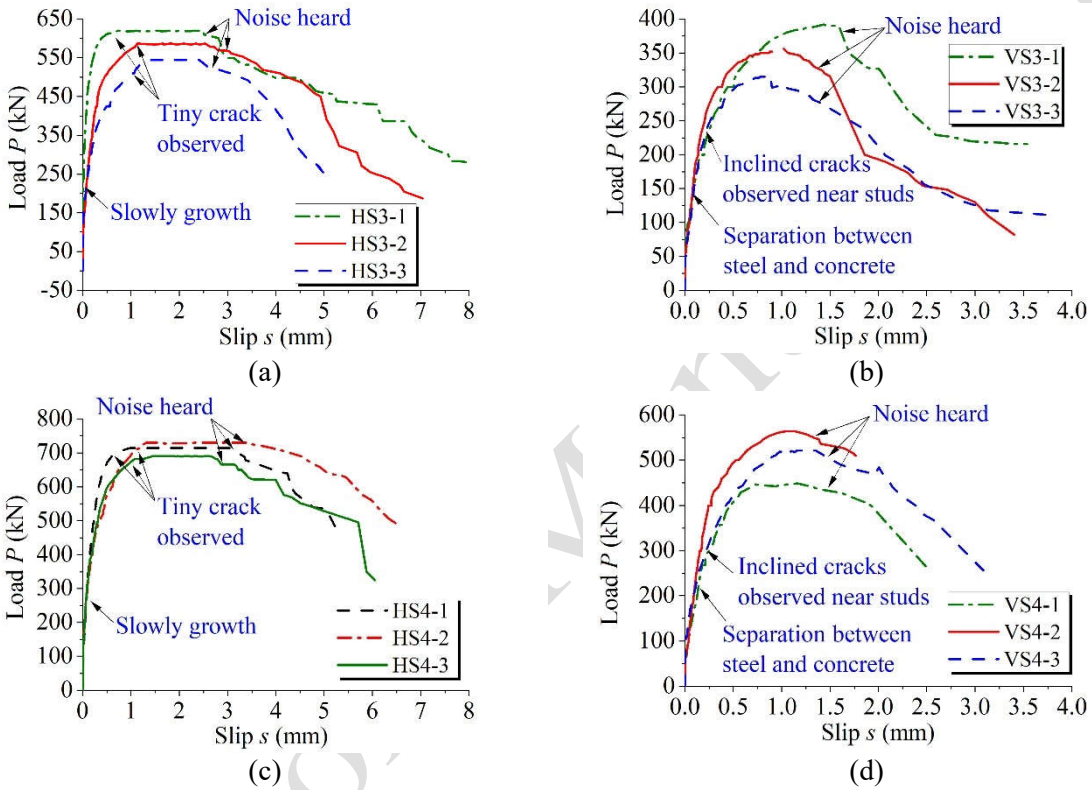

Fig. 6. Load-slip measured from the specimens: (a) HS3; (b) VS3; (c) HS4; (d) VS4.

In the PCSS specimens HS3 and HS4 series, tiny cracks have been observed in the concrete deck after the ultimate load is almost reached. After that, a flat plateau longer than 2 mm can be notably observed on the curve, suggesting the almost zero slope. At the end of the plateau, the fracture-like noise can be heard from the root of studs, suggesting the breaking of studs, as shown in Figs. 6a and c. Following the noise, the load starts to decrease while the slip continues increasing.

In the CSS specimens VS3 and VS4 series, the separation between the concrete and steel has been found at the end of the linear part in the curve. With the load increasing, inclined cracks can be soon found at the concrete near the studs, with a considerable length. Unlike the PCSS specimens, the fracture-like noise has been heard soon after the ultimate load is reached, and no apparent plateau can

be found in the derived curve. After that, the load will decrease at a high rate while the slip continues increasing, as shown in Figs. 6 b and d. The test results reveal that a higher peak load can be reached in the PCSS specimens compared with the CSS specimens. Meanwhile, the load decreases with a very steep slope after the ultimate load in the CSS specimen, compared with the PCSS specimens. In general, the load-slip curve can be divided into three stages according to the curvature, as shown in Fig 7.

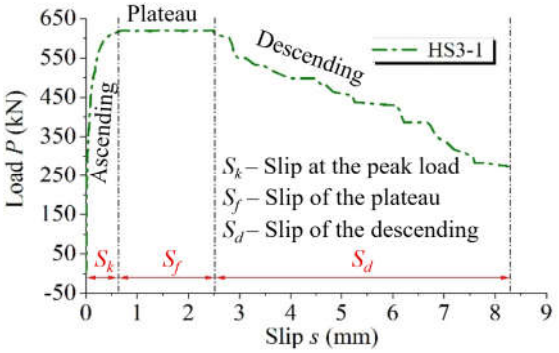

Fig. 7. Division of the load-slip curve (HS3-1).

For better comparison, the ultimate load and slip of each specimen are summarized in Table 4, along with statistics. The ultimate load includes not only the total value at the specimen level but also average per studs. The slip includes from the slip of the peak load S_k, the slip of plateau S_f and the slip of the descending stage S_d. According to the result, the mean ultimate load in the PCSS specimen is about 67.3% higher with 3 rows of studs and 39.1% higher with 4 rows of studs compared with the CSS specimen. Thus, a higher capacity per studs can be reached in PCSS specimens, as shown in Table 4.

Table 4 Summary of ultimate load and slip

Type	ID	Ultimate load P_u (kN)				Slip s (mm)					
		Specimen		Per studs		Peak S_k		Plateau S_p		Descending S_d	
		Test	Mean	Test	Mean	Test	Mean	Test	Mean	Test	Mean
CSS	VS3-1	388		32.3		1.33		-		1.95	
	VS3-2	356	349	29.7	29.1	1.02	1.12	-	-	2.43	2.44
	VS3-3	302		25.2		1.01		-		2.93	
	VS4-1	449		28.1		1.36		-		1.34	
	VS4-2	564	511	35.3	32.0	1.28	1.30	-	-	0.72	1.30
	VS4-3	521		32.6		1.25		-		1.84	
PCSS	HS3-1	620		51.7		0.73		1.75	1.57	5.78	
	HS3-2	587	584	48.9	48.6	1.13	1.23	1.89		4.02	4.18
	HS3-3	544		45.3		1.32		1.08		2.73	
	HS4-1	714		44.6		0.97		2.12	2.08	3.41	
	HS4-2	730	711	45.6	44.5	1.33	1.14	2.08		3.12	3.27
	HS4-3	690		43.1		1.12		2.05		3.27	

Apart from the loading capacity, in terms of the slip, PCSS specimens demonstrate a notably higher ductility compared with CSS specimens. At first, the two types of specimens show a similar slip value at the peak load, i.e. S_k, indicating the similar behaviour before the peak load. However, a very notable slip of plateau S_p could be found in the PCSS specimen, which is hard to be observed from CSS specimens. The mean value of S_p is 1.57 and 2.08 mm in the PCSS specimen with 3 rows and 4 rows of studs, respectively. For further evaluation on the ductility, the slip of descending stage S_d is also derived and listed in Table 4. The average S_d is 2.44 and 1.30 mm in CSS specimens with 3 and 4 rows of studs, respectively. Alternatively, the value is 4.18 mm in PCSS specimens with 3 rows of studs and 3.27 mm in those with 4 rows, which is respectively 1.71 and 2.51 times the value in CSS specimens. Thus, a higher ductility could be expected by using the PCSS.

2.3.2 Failure model

The specimens have been cut after the test to investigate the failure model. Figs. 8a and b show the Macro-sectional view of the PCSS specimen HS4-3 and the CSS specimen VS4-1, respectively. In both types, the failure has been achieved with the studs cut off. However, the fractography in the concrete deck is different in the two types of specimens. In the PCSS specimens, the concrete deck has only been slightly crushed near the root of studs. As shown in Fig. 8a, only a few small cracks can be found around the studs, with a maximum crack width no more than 0.7 mm, and there was no penetrated crack found in all the PCSS specimens.

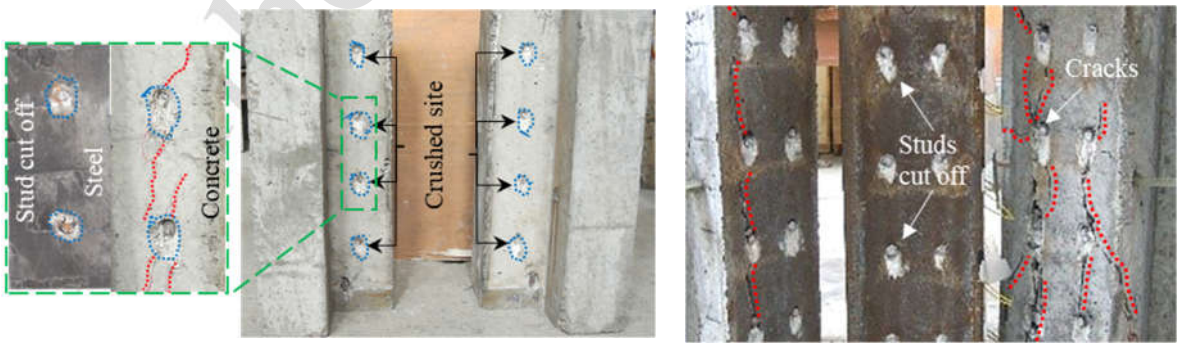

(a) (b)

Fig. 8. Typical Macro-sectional view: (a) PCSS specimen HS4-3; (b) CSS specimen VS4-1.

Alternatively, well-developed cracks can be observed in the CSS specimens, as shown in Fig. 8b. The concrete deck is seriously crushed with the inclined cracks initiated near the studs and propagated to the edge of the deck, with the maximum crack width of 3.5 mm. Meanwhile, most of the cracks in

the CSS specimens have penetrated through the thickness of the deck, and even some have already intersected.

It is worth stating that the section of the concrete deck could be responsible for the significant difference in the failure model between the PCSS and CSS specimens. In this study, the T-shaped deck is employed since it is highly fitted to the configuration of PCSS connectors. For better comparison, it is also used in the fabrication of CSS specimens. However, the volume of concrete around studs is reduced in the CSS specimen with T-shaped deck, compared with the one using the flat deck. As a result, the mechanical performance of near-stud concretes could be decreased in CSS specimen, due to the degradation in the constraint effect by nearby concretes. Thus, once the partial crushing occurred at the root of studs, the concrete around studs would be crushed and cracked at a relatively high rate, while the ultimate capacity would also be soon reached. As reflected on the load-slip curves in Figs. 6b and d, the capacity decreases with a very steep slope after the ultimate load.

2.3.3 Comparison with test data from the literature

For a better understanding of the shear performance of PCSS connectors, further data analysis has been performed on a list of typical push-out test results available from the literature [27]-[34]. Since the PCSS specimen shows a notable difference in the ultimate capacity and the slip of the descending stage, the two indicators have been used in the comparison. It is worth stating that the flat concrete deck was employed in all the investigated push-out tests. The results are visualised in Fig. 9.

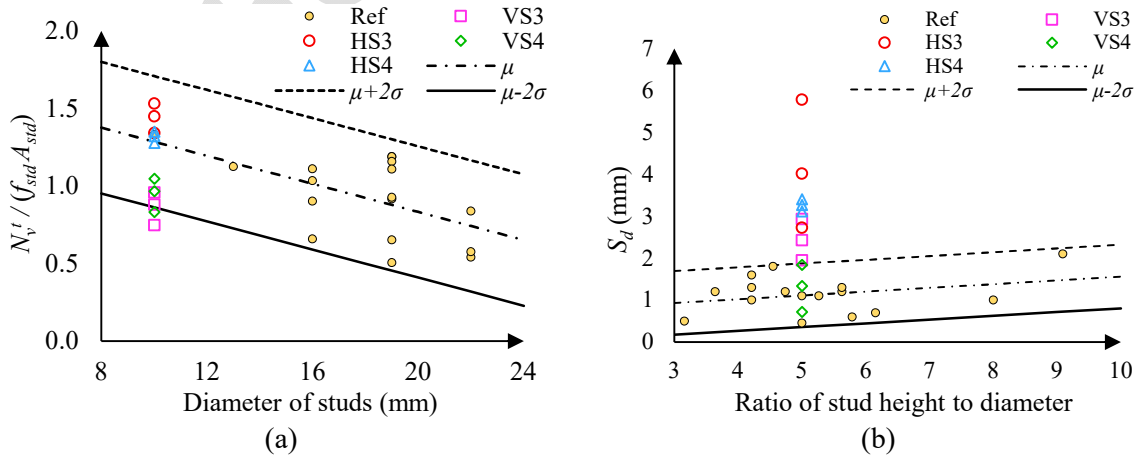

Fig. 9. Comparison between the reference and present test data: (a) Ultimate capacity; (b) slip of the descending stage.

For better comparison, the measured capacity per stud N_v^t has been normalised by dividing the nominal capacity, i.e., the strength f_{std} mutiple the sectional area A_{std}. Besides, the regression line is also derived and included in Fig. 9a, including the mean and the two-sided 97.7% tolerance interval. In the CSS specimen VS3 and VS4, the value falls below the mean and around the lower limit, indicating a lower capacity per studs compared with the flat specimen. On the contrary, the value of PCSS specimen HS3 and HS4 distributed between the mean and the upper limit, suggesting a higher capacity in the PCSS specimen. Above all, the PCSS connector is proven to offer a satisfying capacity along with the enhanced feasibility in prefabricating.

According to Chen and Kunitomo [35], the flexibility is determined by the ratio of the stud height to diameter, i.e., *h/d*. To this end, the slip of the descending stage S_d is plotted against the ratio h/d, as shwon in Fig. 9b. Similarly, the regression lines are derived and plotted, including the mean and the two-sided 97.7% tolerance interval. Except for the test data of VS4 specimens, the measured values are well above the upper tolerance limit. Meanwhile, the PCSS specimens HS3 and HS4 show a notably higher slip S_d compared with the CSS specimens and reference data. As a result, a better ductility and capacity at the descending stage can be achieved by using the PCSS connector.

In terms of the failure model, the traditional specimen is highly similar to the CSS specimen. The failure is mainly induced by the cutting of studs, while cracks initiated in the concrete around the studs and then propagated to visible size when failed. On the contrary, the PCSS specimen demonstrates a notably different failure model, i.e., only the concrete in the vicinity of the studs has been partly crushed with moderate cracks after failed. As a result, a significant plateau could be observed from the corresponding load-slip curves, as shown in Figs. 6a and c.

2.4 Investigation on load transfer mechanism of PCSS specimens

2.4.1 Finite element model

For a better understanding of the load-transfer mechanism of PCSS connectors, a high-resolution finite element (FE) model of the specimen HS4 has been established using the commercial software Abaqus [36], as shown in Fig. 10. In order to downscale the solution cost, the symmetry is utilised so that only half the specimen is modelled. The 3D solid element C3D8R [36] is employed with the

adaptive meshing to balance accuracy and efficiency. The element size is defined as 2 mm in the 50×50 mm region around studs and then gradually increase to 10 mm outside the region.

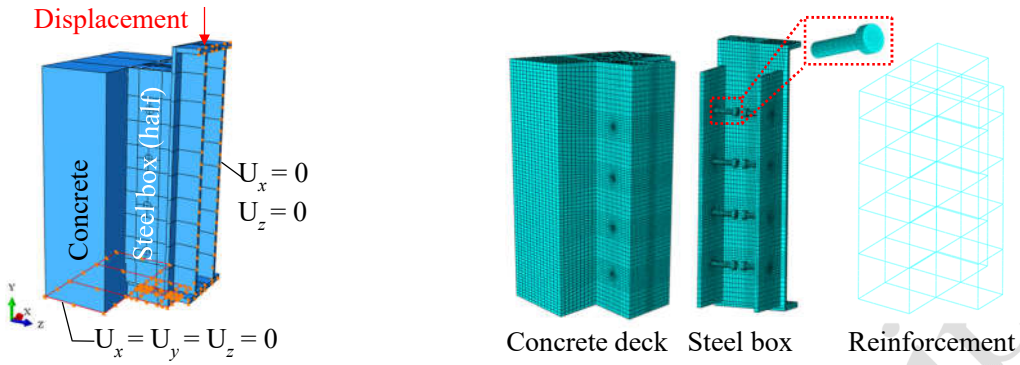

Fig. 10. FE model of HS4: (a) modelling and boundary condition; (b) element and meshing.

The concrete and steel are connected via the "hard contact" algorithm [37], i.e., only the compressive contact force and friction are allowed on the contact surface. In addition, the friction coefficient between concrete and steel is set to 0.6. The loading has been simulated via displacement, of which the maximum is set as 6 mm after the test. Since the FE model includes the complicated nonlinearity in both the material, geometry and contact, the dynamic solver Abaqus/Explicit [38] has been used to keep the solution intractable. Trial calculations have been performed with various loading rates, and the optimal value has been found around 0.6 mm/s, which balances accuracy and efficiency.

2.4.2 Material properties

In simulating material properties of the concrete deck, the concrete damage plasticity (CDP) model is employed as per the suggestion by Nie and Wang [39]. Another crucial aspect of the material model is the uniaxial stress-strain curve, including the compressive and tensile parts. In the compressive part, the empirical equation proposed by Guo [40] has been used, as shown in Equations 2a and b.

$$y = \begin{cases} a_1 x + (3 - 2a_1)x^2 + (a_1 - 2)x^3, & 0 \le x \le 1 \\ \dfrac{x}{a_2(x-1)^2 + x}, & x \ge 1 \end{cases} \quad (2a)$$

$$y = \sigma / f_c \quad , \quad x = \varepsilon / \varepsilon_c \quad (2b)$$

Where σ and ε stand for the stress and strain, respectively; a_1 is the slope factor for the ascending stage, which is set as 1.7 as per [40]; a_2 is the slope factor for the descending stage, which is set as 2.0 as per [40]; f_c is the uniaxial compressive strength, respectively; ε_c is the reference strain at the peak stress, set as 0.002 according to [40].

The cubic strength f_{cube} is determined from the material test as shown in Table 2, while the uniaxial strength f_c is determined as $0.76f_{cube}$ [41]. Meanwhile, the maximum compressive strain is determined as 0.0035 [40]. Besides, the Poisson's ratio of the concrete is determined as 0.2 [41]. In the tensile part, the linear simplification [42] has been used, i.e., the stress increases proportionally with the strain until the ultimate tensile strength f_t is reached. After that, the stress is released from the cracked concrete and re-distributed to the nearby part. According to [41], the uniaxial tensile strength f_t could be derived based on the cubic compressive strength f_{cube}, as shown in Equation 3.

$$f_t = 0.395 f_{cube}^{0.55} \tag{3}$$

Thus, the uniaxial strain-stress relation of the concrete is derived, as shown in Figs. 11a and b.

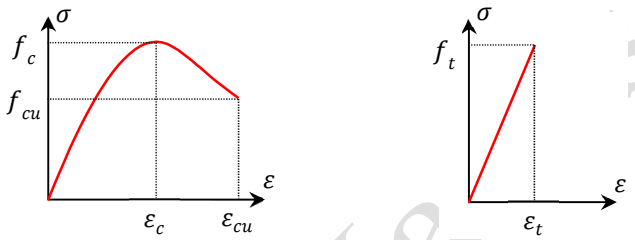

Fig. 11. Uniaxial stress-strain curve of the concrete: (a) Compression; (b) Tension.

In the case of the steel, the trilinear model with hardening is applied to steel studs, as shown in Fig. 12a, including the yielding strength f_y and strain ε_y, and the ultimate strength f_u and strain ε_u. Meanwhile, the bilinear model is used for the steel box and reinforcement, as shown in Fig. 12b, with the properties f_y and ε_y only. Besides, the Poisson's ratio of the steel is set to 0.3 according to [43].

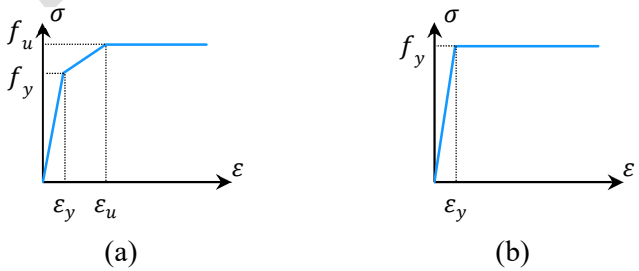

Fig. 12. Constitutive model of the steel: (a) Trilinear; (b) Bilinear.

2.4.3 Numerical results and discussion

The predicted load-slip curve calculated from the FE model is shown in Fig. 12, combined with the test curves. Overall, the FE result is in good agreement with the test data. In the elastic stage when $P < 0.5P_u$, the slip increases proportionally with the load while little discrepancy could be found

between the FEM and test, i.e., no more than 4.7%. As the load increase beyond 50% of the peak load, a slight discrepancy occurs between the FE prediction and test result. As the loading continues, the FE model reached its ultimate capacity of 725 kN, which is 2.0% higher than the measured mean capacity of 711 kN. Meanwhile, the predicted slip at the peak load is 1.32 mm, i.e., about 15% higher than the measured mean. Besides, a high similarity could also be found in the slip of plateau S_f, which is 2.05 mm from test and 2.08 mm by the FE (only 1.4% difference). After that, the slip increases while the load keeps decreasing, i.e., the descending stage. Finally, the FE model failed at the load of 420 kN due to convergence difficulties. A visible difference can be found between the FE and test curves, but the trend is still highly similar.

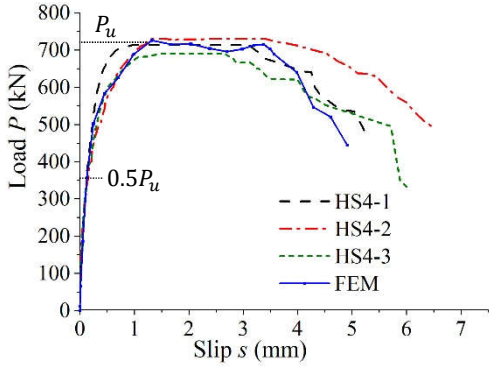

Fig. 13. Comparison of load-slip curves between test and FE model

Further comparison is carried out on the crushing state of concretes at the failure state between the FE model and the specimen HS4-2, as shown in Figs. 14a and b. The FE results are presented in terms of damage factor indicating the crushing state of concretes. The comparison also suggests a good match in the failure state between the test and FE prediction. Thus, the established FE model is able to reflect the behaviour of the push-out tests.

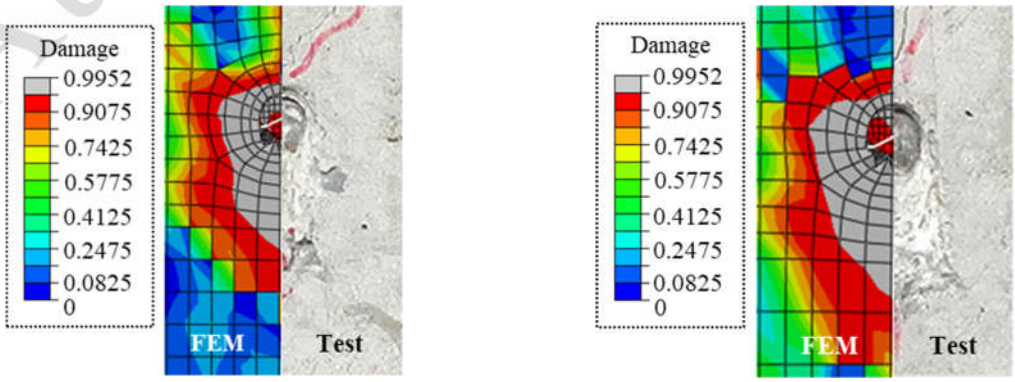

Fig. 14. Comparison of concrete crushing between HS4-2 and FE model: (a) Concrete near the 2nd row of studs; (b) oncrete near the 3rd row of studs.

Based on the verified FE model, the load transfer mechanism in the PCSS is investigated in terms of damage in the concrete and Von Mises stress in the stud, as shown in Fig. 15. Generally, the loading process can be divided into 4 phases by 4 points on the load-slip curve. Before loaded to 363 kN (about 50% the peak load), the specimen demonstrates almost perfectly linear behaviour on the load-slip curve. Accordingly, no obvious damage could be identified at the concrete, and the stud stress is well below the yield strength. Once loaded to 363 kN (about 50% the peak load), the concrete damage starts to initiate near the root of studs, as shown by the grey part in Point (1). Meanwhile, the maximum stud stress reaches 335 MPa, very close to the yield strength of 340 MPa. However, the interaction between the stud and concrete is still fully active due to the very limited concrete damage.

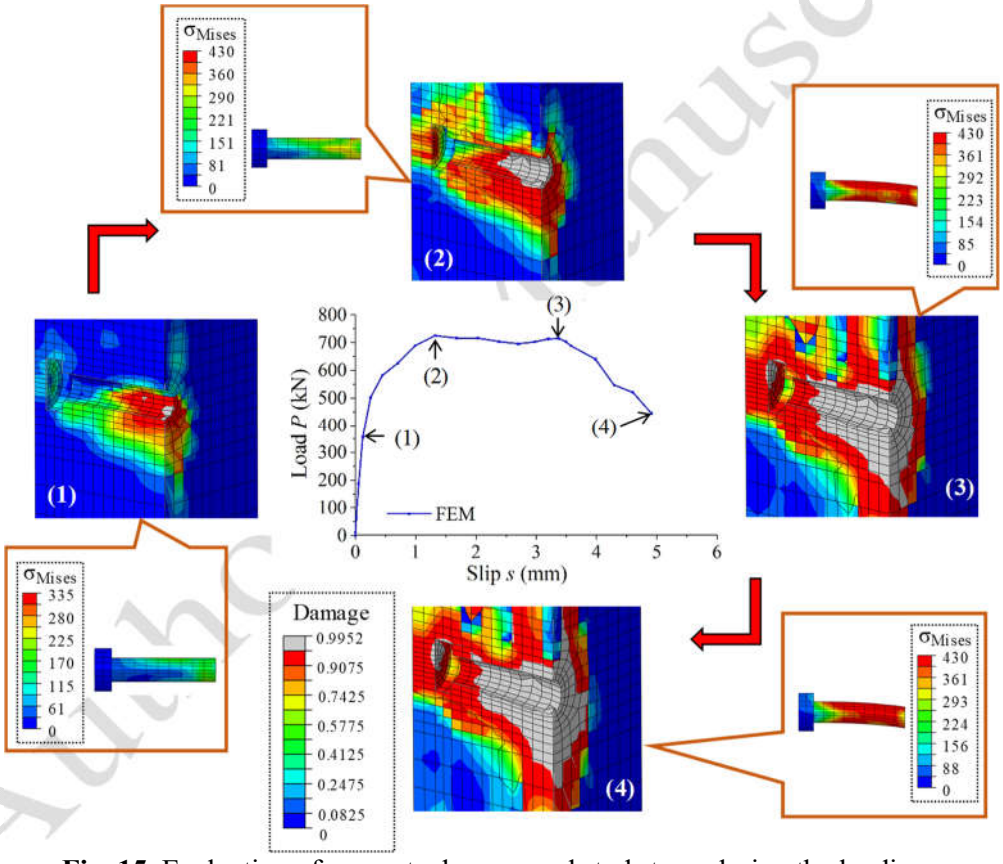

Fig. 15. Evaluation of concrete damage and stud stress during the loading.

With further loading, the proportion of crushed concrete increases, and the studs gradually begin yielding. As a result, notable nonlinearity can be observed on the load-slip curve. Once loaded to the peak value of 725 kN, as shown by Point (2), the crushed concrete becomes interconnected around the hole. However, the diameter of the crushed region is only about 1.5 mm. Moreover, a small part of studs reaches the yielding and even ultimate strength. In general, although the stud yielding and concrete

crushing occur in the PCSS specimen at this stage, a good interaction still exists between the stud and concrete. This is highly similar to the traditional stud connector. As a result, the PCSS connector behaves like the traditional stud before the peak load.

After that, the load-slip curve shows a plateau until Point (3). Between Points (2) and (3), the slip increases by almost 171%, while the crushed concrete region extends from 1.5mm to 4.5 mm in diameter. Besides, most part of the stud reaches the ultimate strength at Point (3). The notable plateau can be attributed to the lateral constraint on the concrete by the two vertical steel plates. With the constraint, both the ultimate strength and ductility are enhanced for the concrete within the plates. Thus, the stud-concrete interaction still lasts for a notable time period even after the ultimate of studs has been achieved. As a result, the remarkable plateau can be observed on the load-slip curve before the final fracture of studs. After Point (3), most part of the stud reaches the ultimate strength. Thus, the load capacity of the specimen degrades, reflected by the descending load-slip curve. However, it is very interesting that the volume of crushed concrete stays almost stationary until the failure. This could be attributed to the lateral constraint on the concrete offered by the vertical steel plate. Thus, the specimen still shows a considerable remnant capacity during the descending stage.

In order to further explore the lateral constraint effect on the concrete, the out-of-plane normal stress has been derived for the vertical plate near the stud, as shown in Figs. 16. According to the result, inter-extrusion between the concrete and vertical steel plate, and the stress increase with the slip until the final failure. As a result, the lateral deformation of the concrete is constrained by the vertical steel plate, which in turn help to control the proportion of crushed concretes around studs. As a result, a notable slip could be observed in the descending stage of the load-slip curve.

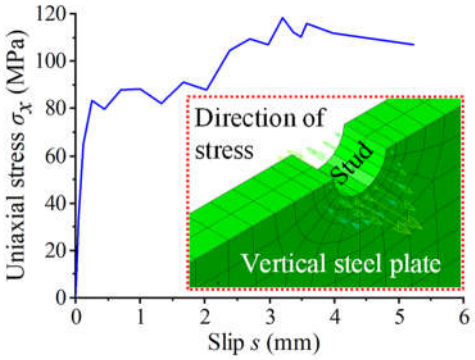

Fig. 16. Out-of-plane normal stress of the vertical steel plate near studs.

3. Investigation on the prefabricated composite bridges using the PCSS

3.1 Full-scale model test of the composite bridge using PCSS

A full-scale model test of the prefabricated steel-concrete composite bridge has been employed to investigate the mechanical behaviour of prefabricated composite bridges using the PCSS, as shown in Figs. 17 and b.

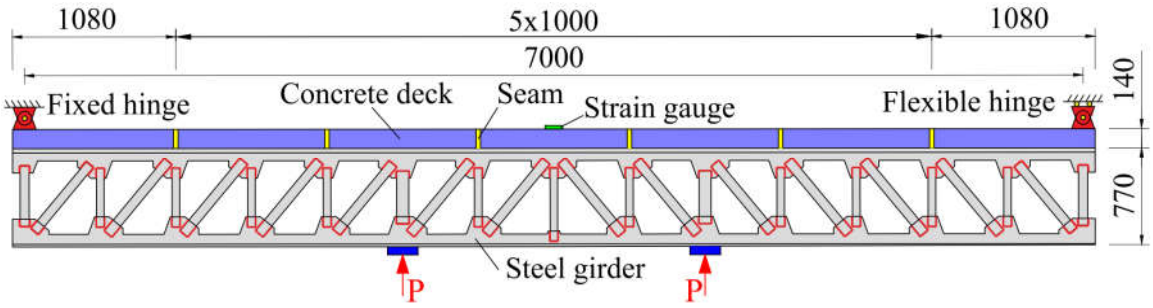

(a)

(b)

Fig. 17. Full-scale test of the prefabricated composite specimen: (a) Elevational view (Unit: mm); (b) Photograph.

The specimen consists of a steel truss girder and a pre-cast concrete deck prestressed by tendons. The PCSS connector has been employed to connect the deck and the top flange of the upper chords in the truss. The specimen is simply supported with a span of 7000 mm. Two actuators working in-phase have been used to load the specimen from bottom-up, through which the negative bending moment is simulated. Meanwhile, a strain gauge is installed on the top surface of the concrete at the mid-span, as shown in Fig. 17a.

The materials used in the full-scale test have been kept the same as those employed in the previous push-out test, as listed in Table 2. Besides, the prestress is applied on the deck through the steel tendon $1\phi^s15.2$-1860 [25], of which the ultimate strength is 1860 MPa. In the prefabrication, the deck has been divided into 7 blocks, each of which is 1000 mm in length. The PCSS connector is embedded in the deck blocks when casting, with a total of 28 studs in a single block. After that, the deck blocks with the PCSS embedded are integrated through preloading the steel tendons. The Grade-A binder [44] has been

injected into the seams between deck blocks before applying the prestress to improve the integrity of the deck. The elastic modulus of the binder is 3200 MPa. Its tensile and compressive strengths are 8.5 and 50 MPa, respectively. More details about the binder can be found from the reference [44].

Before loading, the tendons are preloaded to 1395 MPa from the two ends using the hydraulic jacks. Three hours after the preloading, the top-surface strain of the deck has been measured via the gauge shown in Fig. 17a, which is -650 με. Three loading phases have been conducted on the specimen during the test, and the results are illustrated in Figs. 18a to e. In the first phase, the specimen is loaded and unloaded for three cycles under the load of P = 180 kN. Overall, the specimen demonstrates the elastic behaviour, and no apparent crack has been found. Also, the strain on the top surface of the deck is measured as -182 με, indicating enough remnant prestress and compressive state of the deck. As a result, the deformation and stress increase and decrease linearly with loading and unloading.

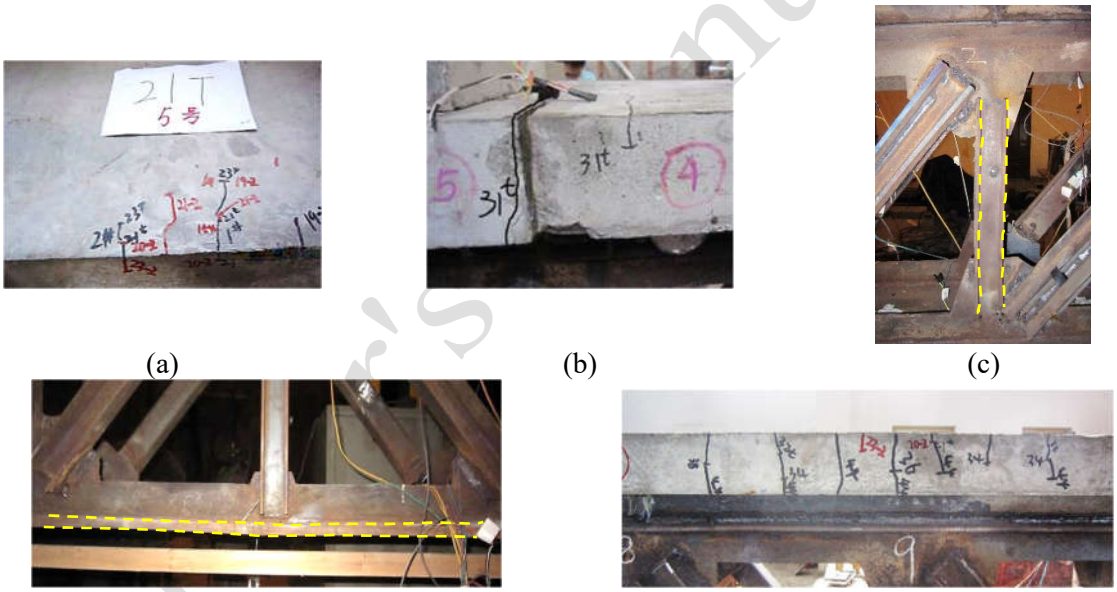

Fig. 18. Test result of the prefabricated composite specimen: (a) The first crack at the deck viewed from top; (b) The first crack at the seam viewed from elevation; (c) buckling of the vertical member near the bearing; (d) buckling of the lower chord at the midspan; (e) the longitudinal welded joint at the failure stage.

In the second phase, the specimen is at first loaded to P = 210 kN. At the same time, the top-surface strain becomes 18 με, suggesting the prestress is completely eliminated by the external load. Thus, two cracks have been soon observed at the top surface of the deck near the loading site, as shown in Fig. 18a, including the 1st crack marked as "1#" and the 2nd crack marked as "2#". However, crack closure occurred at the observed cracking site directly after unloading.

At the third phase, the specimen is directly loaded until failure and the peak load attained is recorded as the ultimate load, i.e., P = 500 kN. As the load increases to 310 kN, the first crack at the seam has been observed, as shown in Fig. 18b. After that, cracks extensively initiate at the seams and propagate much faster than the cracks within blocks. Finally, when the load increases to 500 kN, buckling can be found at the vertical member, as shown in Fig. 18c, and the lower chord, as shown in Fig. 18d. At the same time, the three deck blocks near the midspan are seriously cracked and split. Since the load could not be increased anymore, the failure of the specimen is identified at the ultimate load of 500 kN, and the test is stopped. It is worth noting that the longitudinal welded joint between the PCSS and truss has stayed intact during the whole loading process. As shown in Fig. 18e, no visible damage could be found in the longitudinal welded joint when the failure of the specimen has occurred. On this end, the feasibility is further verified for the longitudinal welded joint of PCSS connectors in prefabricated composite bridges.

3.2 Establishment of the numerical model

3.2.1 Element and meshing

An advanced finite element (FE) model has been established for the full-scale prefabricated composite specimen using the software Abaqus [36], as shown in Fig. 19. The concrete deck and PCSS connectors are modelled with the solid element C3D8R, while the truss element T3D2 is used to simulate the prestress tendons and reinforcements. In the steel truss girder, the structural members are modelled with the shell element S4R. In the full-scale test, the binder was used to connect the deck blocks at the seam. Since the binder's tensile strength (8.5 MPa) is favoured to the capacity, it is not explicitly modelled. Instead, the seam is simulated by a 10 mm-wide concrete segment without reinforcement for conservativeness.

The details of element selection are also included in Fig. 19. Different meshing sizes have been employed for the various components to ensure both the accuracy and computational feasibility, as shown in Fig. 20. A relatively coarse meshing size is used for the shell elements simulating the steel truss girder, i.e. 20 mm since it is not of special interest. The deck is modelled by the C3D8R with a size of 8 mm. Accordingly, the PCSS connectors are discretized with a refined meshing size ranging from 4 mm to 8 mm. For the seams between blocks, the meshing size of 5 mm is used to ensure the

sufficient layer of solid elements. A coarse meshing size, i.e. 37 mm, has been applied in modelling the prestress tendons and reinforcements since they are mainly used to integrate the deck.

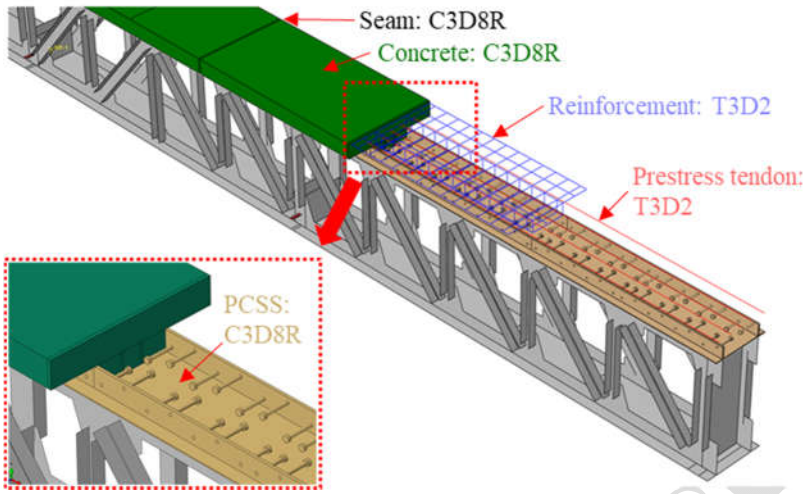

Fig. 19. Advanced FE model of the prefabricated composite specimen.

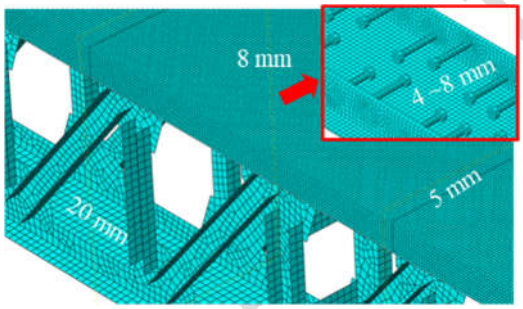

Fig. 20. Meshing of the advanced FE model.

3.2.2 Contact relation, boundary condition and material models

The deck is connected with the prestress tendons and reinforcements using the "embedding" hard contact [36], i.e. the displacement-interpolation. Meanwhile, the welded joint between the top surface of the truss and the vertical plates of PCSS connectors are modelled through the "tie" contact [36], i.e. the displacement-coupling. Between the concrete and studs, the face-to-face hard contact has been applied, and the friction coefficient is set as 0.6 according to [37].

The boundary conditions of the FE model are set in accordance with the actual situation of the prefabricated composite specimen shown in Fig. 17. The loading procedure has been simulated through imposing a total displacement of 50 mm. Similarly, the solution has been carried out through the quasi-static analysis using the Abaqus/Explicit dynamic solver to ensure computational efficiency. At first, an artificial duration of 50 seconds is adopted for loading to failure, and the loading rate is accordingly

determined as 1 mm/second. After that, the adjustment is made to balance the efficiency and accuracy through trial computations, using the procedures illustrated in section 3.2.

The material properties and models employed in section 2.4 have been adopted in the FE simulation of the full-scale specimen, including the stud, steel plates and concrete since the materials in the full-scale test are kept the same as in the push-out test. Besides, the prestress tendon has been regarded as the elastic material since the used steel wire has no clear yielding point, and it stayed intact until the failure of the specimen.

3.3 Verification of the FE model

The load-deflection curves obtained from the test and the numerical simulation are compared in Fig. 21. When the load is below 56% of the ultimate load, i.e. $0.56P_u$, the prefabricated composite specimen mainly demonstrates the linear elastic behaviour, and the FE curve matches very well with the measured curve. For instance, under the load of 250kN, the displacement measured at the mid-span of the specimen is 12.33 mm, while the corresponding FE value is 12.50 mm, i.e., about 1% error. As the load further increases beyond $0.56P_u$, the curve gradually shows the notable nonlinearity, indicating the elastic-to-plastic behaviour of the specimen. After loaded to $0.9P_u$, the mid-span deflection of the specimen is 38.03 mm, while the FE value is 34.69 mm, i.e., an error of 8.7%. However, this difference is somehow acceptable, considering the complexity in modelling nonlinear behaviour.

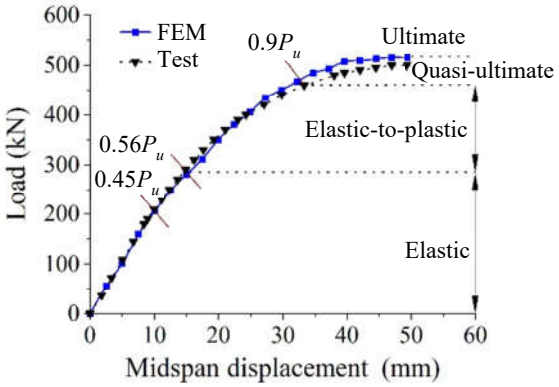

Fig. 21. Load-displacement curve of the prefabricated composite specimen.

Overall, the derived load-deflection curve from FEM keeps in good agreement with test data. Besides, the FE model also matches well with the test respecting the distribution of cracks and the failure mode, which will be discussed in detail in the following section. To sum, the FE model is validated by the test data.

3.4 Numerical Results

3.4.1 Classification of loading stages

As shown previously in Fig. 21, the mechanical behaviour of the prefabricated composite specimen can be divided into three phases, including the elastic, elastic-to-plastic and quasi-ultimate stages. At the elastic stage ($P < 0.56P_u$),the load-deflection curve shows a linear trend. As the load increased to $0.45P_u$ (i.e., 210kN), notable tensile stress could be observed at several points on the deck top surface, suggesting that the prestress is counterbalanced by the applied load. As a result, the first crack occurs at the deck surface. However, the specimen still demonstrates elastic behaviour since the load and deformation are almost in a linear relation.

At the elastic-to-plastic stage ($0.56P_u < P < 0.9P_u$), the prestress effect is entirely eliminated by the load. In this situation, the deck works in the way of the reinforcement concrete (RC) member. As a result, the load-displacement curve is no longer linear, but the change in slope is moderate. As the load further increased to $0.62P_u$ (i.e., 310kN), the 1st cracking occurs at the seam close to the midspan, as shown in Fig. 22. In RC members, the crack size would be directly controlled by the reinforcement ratio. Since no reinforcement passes through the seam, the cracking-resistance becomes lower at the seam compared with the pre-cast blocks. With the load further increasing to $0.76P_u$ (i.e., 380 kN), the 2nd cracking site appears at the seam near the midspan, as shown in Fig. 22. Along with the crack, an abrupt change could be observed on the load-slip curve. At the quasi-ultimate stage ($P > 0.9P_u$), the load-displacement curve gradually becomes flat, and the deformation increases rapidly with the load.

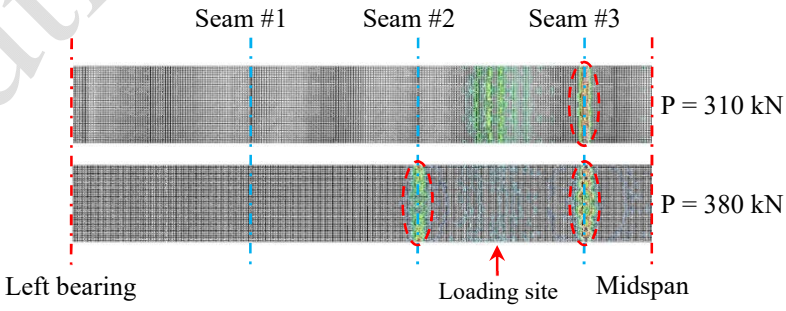

Fig. 22. Cracking site on the concrete deck

3.4.2 Stress and crack distribution at the ultimate stage

Figs. 23a and b respectively show the ultimate stress state and crack distribution from the FE model. The result suggests that the yield stress is reached in a considerable proportion of the truss members,

especially in the web members and lower chords. Fig. 23b shows the distribution of cracks in the deck, in which the coloured parts indicate the cracked location. It can be found that cracks have already been fully developed in the three deck blocks near the midspan, similar to the cracks in the test specimen. Besides, the cracking at the seams between deck blocks is much more severe than that within the blocks.

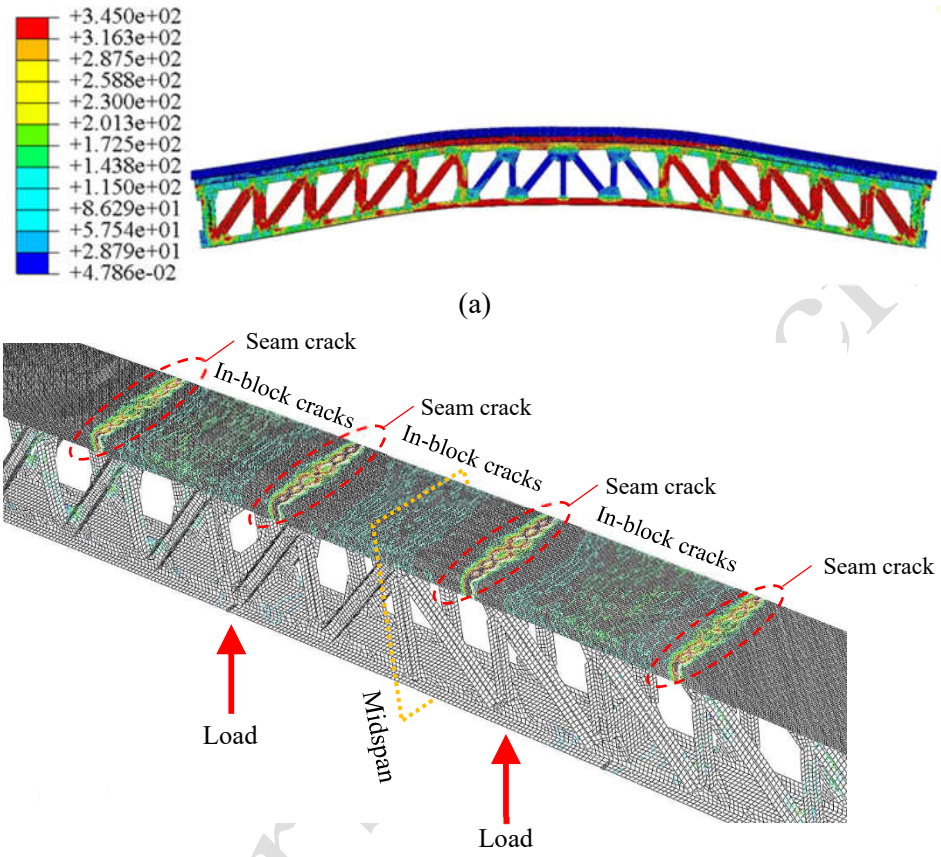

Fig. 23. FE result at the ultimate state: (a) Von Mises stress (MPa); (b) Crack distribution.

3.4.3 Distribution of slip at various stages

The slip between the deck and stud is calculated at the stud root, and the mean value from the studs with the same longitudinal position has been employed. Fig. 24 shows the representative distribution of the slip at three loading stages, including of the elastic stage, elastic-to-plastic (E-to-P) stage and quasi-ultimate (QU) stage. The result shows significant differences between the three stages. At the load of $0.45P_u$, i.e. the elastic stage, the slip is varied smoothly with the distance. Since the load increases to $0.56P_u$ at the E-to-P stage, the specimen demonstrates the elastic-to-plastic behaviour, and abrupt changes can be found in the distribution. After that, the abrupt change escalates with the increase in the load. As the load further grows to $0.9P_u$ at the quasi-ultimate stage, the abrupt changes become very remarkable, and sharp step changes can even be found at several points.

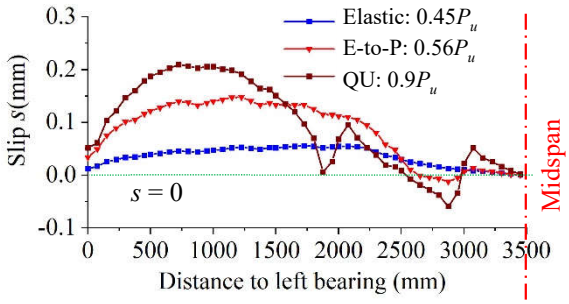

Fig. 24. Longitudinal distribution of the slip at different stages

During the elastic stage, the slip of PCSS connectors shows a continuous distribution, as shown by the blue line in Fig. 24. The slip is relatively small at the bearing, and then gradually increases with the distance until the loading point is reached. For better illustration, Figs. 25a and b show the corresponding displacement of studs in the shear-bending zone and pure bending zone, respectively. In the shear-bending zone, i.e. the zone from the bearing to the loading point, the displacement of studs increases with the distance, as shown in Fig. 25a. In the pure bending zone between the two loading points, symmetry trend can be observed. Especially, the displacement of studs gradually decreases to zero from the loading point to the midspan, as shown in Fig. 25b.

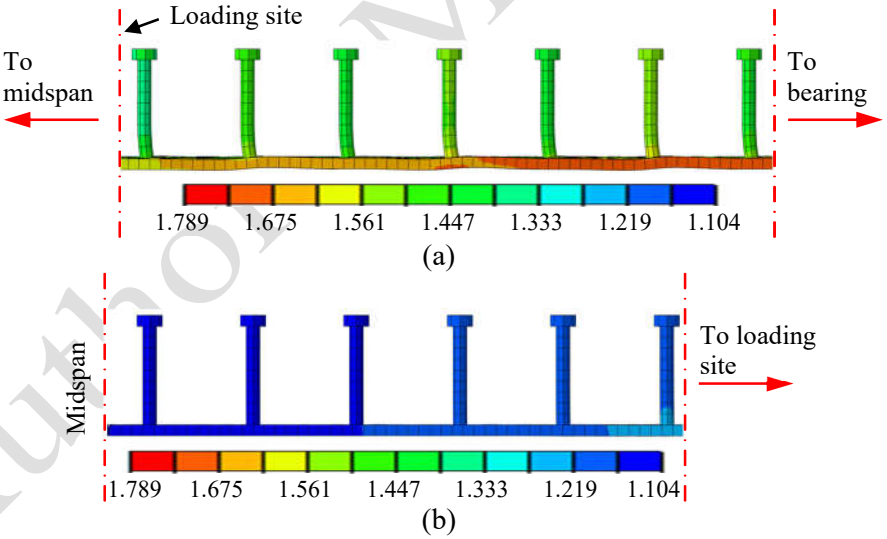

Fig. 25. Displacement of studs at 0.45P_u (Unit: mm): (a) shear-bending zone; (b) pure bending zone.

When the load increase increases to 0.56P_u, cracks initiate at the seam between deck blocks, as shown in Fig. 26. As a result, the slip is no longer continuously distributed. Fig. 26 also includes the displacement of studs near the seam crack, i.e. l = 3000 mm. The result suggests that the displacement decreases to zero at the cracking site of the seam, and then symmetrically increases with the distance. This effect can be related to the first zigzag in the slip shown in Fig. 26.

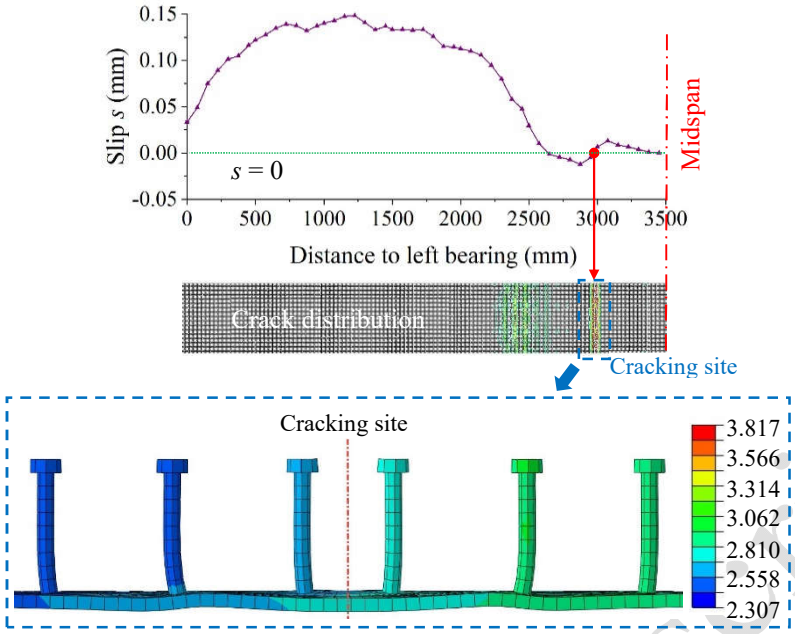

Fig. 26. Slip and stud displacement at $0.56P_u$ (Unit: mm).

As the load further increases beyond $0.56P_u$, the specimen demonstrates elastic-plastic behaviour, and both the width and number of cracks continue to grow. Fig. 27 show the crack distribution and slip at the load of $0.9P_u$. The result suggests the concentration of cracks in the three deck blocks near the midspan, with the maximum cracking width at the seams. The slip of studs reduces to almost zero at the two cracked seams near l=1800 mm and l=3 000 mm, as shown in Fig. 27. Similarly, the abrupt change can be observed at the two cracking sites in the slip, with an escalated scale.

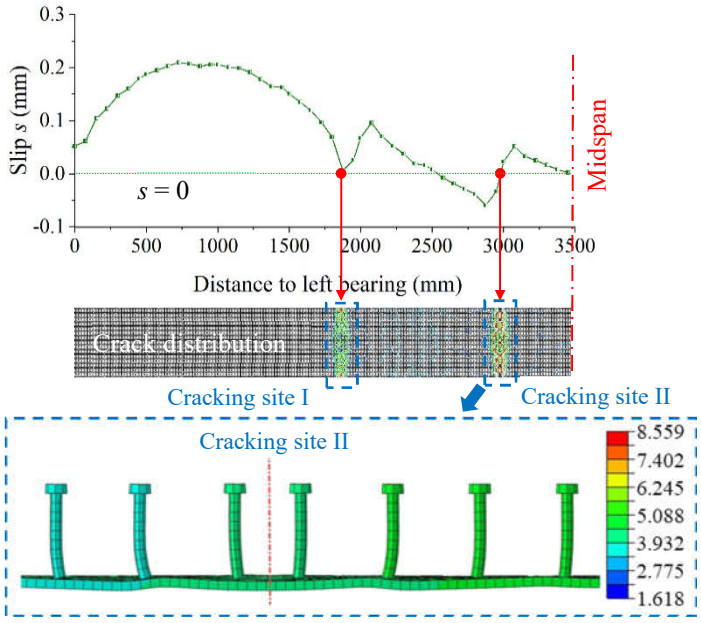

Fig. 27. Slip and displacement at $0.9P_u$ (Unit: mm).

When the load increase beyond 90% of the ultimate load, the cracks extensively develop, while the three decks in the midspan gradually cease to work. Meanwhile, the lower chord of the steel truss girder gradually yielded. At this stage, the abrupt increase can also be found in the slip of the studs near the cracked seams, as shown in Figs. 28a and b. Finally, the ultimate capacity is achieved since no additional load can be applied to the specimen.

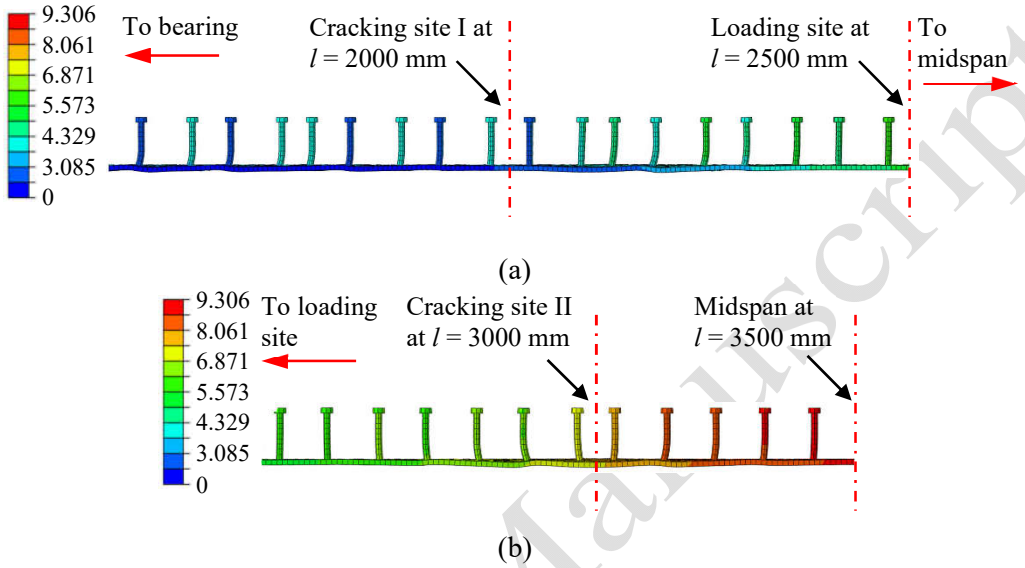

Fig. 28. Displacement of studs at the ultimate state (Unit: mm): (a) shear-bending zone; (b) pure bending zone.

3.5 Discussions on the numerical result

The slip distribution is also closely related to the configuration of the deck and the cracking feature of the prefabricated composite specimen. As described in section 3.1, once the crack initiates at the seam (P = 310 kN), it will develop at a much higher rate, and gradually become the major cause for the final failure of the specimen. This is mainly because the reinforcement is embedded within the deck blocks but no at the seam. Thus, the bond-slip theory [45] is used to illustrate the mechanism of shear-slip transfer between the concrete and steel, as shown in Fig. 29.

As the growth of cracks in the concrete, the stress at the cracked parts is gradually released from $\sigma_{p0} + \sigma_{ct}$ to 0, in which σ_{p0} is the prestress and σ_{ct} is the concrete stress. Accordingly, the released stress will be re-distributed to the nearby components, including the prestress tendons, truss members and uncracked concretes. The released stress increases from zero at the cracked seam to a peak value at a certain distance from the crack and then decreases to zero again with the distance. As a result of the stress redistribution, an additional slip Δs will be induced between the concrete and steel near the

603 cracked seam. Similar to the stress redistribution, the additional slip reaches its peak at a certain distance
604 from the cracked seam and then falls back to zero with the distance. Consequently, the abrupt changes
605 could be found in the distribution of slip along the girder.

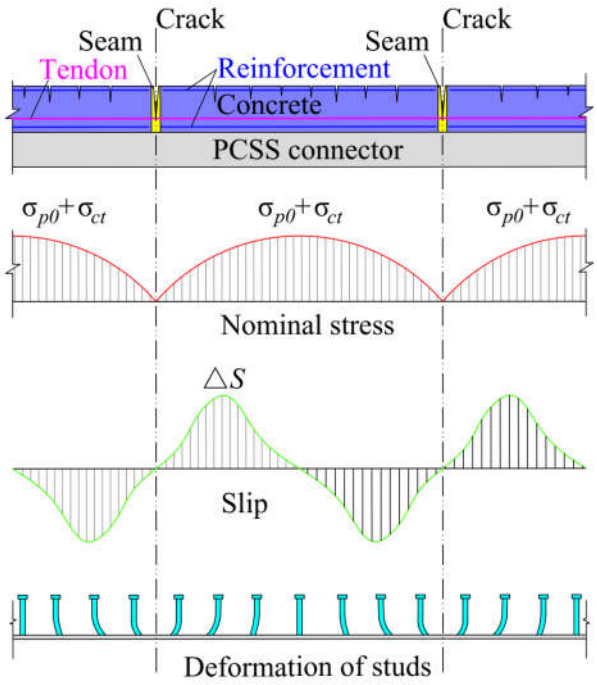

606
607 **Fig. 29.** Redistribution of stress and slip in the PCSS specimen after cracking at the seam.

608 **4. Conclusions**

609 In this paper, a series of experimental and numerical works have been carried out to investigate the
610 load-slip behaviour of an innovative prefabricated shear stud (PCSS) connector and its application in
611 the prefabricated steel-concrete composite bridges. The following conclusions can be drawn:

612 ● Push-out tests have been performed on a total of 12 specimens, including 6 PCSS specimens and 6
613 specimens with the conventional shear stud (CSS). Overall, the ultimate capacity of the PCSS
614 specimen is about 39.1%-67.3% higher than the CSS specimen. Meanwhile, the PCSS specimen
615 shows the notable "flat plateau" and descending stage on the load-slip curve after the peak load,
616 which ensures a much better ductility. Besides, the concrete was just slightly crushed near the stud
617 root in PCSS specimens, compared with the well-developed cracks in the CSS specimens.

618 ● Comparison has also made between the test result and the data from the literature, in which the flat
619 concrete deck was used, in terms of the capacity per studs and slip of descending stage. According
620 to the result, the normalised stud capacity of the PCSS specimen falls between the mean value and

upper tolerance limit derived from the literature, further indicating a satisfying capacity of PCSS specimens. Meanwhile, the slip of the descending stage in the PCSS specimen is well above the upper limit by the literature, suggesting a better ductility. To sum, the PCSS connector enables the full prefabrication of composite bridges without compromise in the capacity and ductility.

- A high-resolution FE model has been established for the PCSS specimen and validated through the test data. Based on the model, the investigation is performed to investigate the load transfer mechanism of the PCSS connector at the component-level, including the stress of studs, damage of concretes, and stress state of vertical steel plates. The result reveals that the ultimate capacity of the PCSS is mainly controlled by the yielding of studs. However, the surrounding concrete could provide an effective constraint on the studs after they yielded, leading to the notable plateau and descending stage in the load-slip curve. At the same time, the damage of concretes is limited by the lateral constraint from vertical steel plate, resulting in a remarkable improvement in ductility of the PCSS specimen.
- A full-scale model test is employed to verify the application of PCSS connectors in prefabricated composite bridges. Based on the test, an advanced FE model has been established for the specimen and validated using the test data. The result shows that the slip distribution is influenced by the cracking at the seam between prefabricated deck blocks. As a result, the abrupt changes can be found in the load slip curve after cracking occurs, which differs from the traditional composite bridges.

Acknowledgements

The research is supported by the National Natural Science Foundation of China (Project No: 51778094), the Natural Science Foundation of Chongqing City, China (Grant No. cstc2018jcyjAX0509, cstc2020jcyj-msxm1602) and the Science and Technology Project of DOT of Yunnan Province, China (Project No: 2018-28).

Conflict of Interest

There is no conflict of interest associated with this publication.

Data Availability Statement

All the data, model or code data employed in the study appear in the submitted paper.

649 **References**

650 [1] Johnson, R.P., Composite structures of steel and concrete: beams, slabs, columns, and frames
651 for buildings, 3rd edition, John Wiley & Sons, Hoboken, US, 2008.
652 [2] Hällmark, R., White, H., & Collin, P. (2012). Prefabricated bridge construction across Europe
653 and America, PRACT. PERIOD. STRUCT. DES. CONSTR., 17(3): 82-92.
654 https://10.1061/(ASCE)SC.1943-5576.0000116 10.1061/(ASCE)SC.1943-5576.0000116
655 [3] Chaudhary, S., Pendharkar, U., & Nagpal, A. (2009). Control of creep and shrinkage effects in
656 steel concrete composite bridges with precast decks, J. BRIDGE ENG., 14(5): 336–345.
657 https:10.1061/(ASCE)1084-0702(2009)14:5(336)
658 [4] Ehab, E., & Dennis, L. (2002). Modelling of headed stud in steel-precast composite beams,
659 STEEL COMPOS. STRUCT., 2, No. 5, 355-378. https://doi.org/10.12989/scs.2002.2.5.355
660 [5] Shim, C.S., Chung, C.H., Kim, I.K., & Kim, Y.J. (2010). Development and Application of
661 Precast Slabs for Composite Bridges, STRUCT. ENG. INT., 20(2): 126-133.
662 https://doi.org/10.2749/101686610791283623
663 [6] Huang, D., Wei, J., Liu, X., Xiang P., & Zhang, S. (2019). Experimental study on long-term
664 performance of steel-concrete composite bridge with an assembled concrete deck, CONSTR
665 BUILD. MATER., 214: 606–618. https://doi.org/10.1016/j.conbuildmat.2019.04.167
666 [7] Nijgh, M. P., Gîrbacea, I. A., & Veljkovic, M. (2019). Elastic behaviour of a tapered steel-
667 concrete composite beam optimized for reuse, ENG. STRUCT., 183: 366–374.
668 https://doi.org/10.1016/j.engstruct.2019.01.022
669 [8] Mirza, O., Kaewunruen, S., Kwokand, K., & Griffin, D.W.P. (2016). Design and modelling of
670 pre-cast steel-concrete composites for resilient railway track slabs, STEEL COMPOS.,
671 STRUCT., 22(3): 537-565. https://doi.org/10.1016/j.istruc.2019.03.006
672 [9] Shim, C S., Jeon, S.M., & Kim, D.W. (2008). Evaluation of static strength of group stud shear
673 connection in precast concrete deck bridges, BRIT. MED. J., 20(2): 672-684.

[10] Xiang, Y., GUO, S., Zheng, Q., Chen, Z., & Lin, H. (2017). Influence of Group Studs Layout Style on Static Behavior of Steel-Concrete Composite Small Box Girder Models， J. BUILD. STRUCT., 38(s1):376-383. https://doi.org 10. 14006/j. jzjgxb. 2017. S1. 053

[11] Wang, Y., Yu, J., Liu. J., & Frank, Y. (2019). Shear behavior of shear stud groups in precast concrete decks, ENG. STRUC., 187: 73–84. https://doi.org/10.1016/j.engstruct.2019.02.002

[12] Sjaarda, M., Porter, T., West, J.S., & Walbridge, S. (2017). Fatigue Behavior of Welded Shear Studs in Precast Composite Beams. J. BRIDGE ENG., 22(11): 04017089. https://doi.org/10.1061/(ASCE)BE.1943-5592.0001134.

[13] Liu, M., Wan, J., & Zhang, Q. (2014). Mechanical Analysis of a Steel-concrete Composite Girder Bridge under Cluster Distribution and Uniform Distribution of the Shear Studs, J. CIVIL ENG. MANAG., 31(3):1-6. https://doi.org/10.13579/j.cnki.2095-0985.2014.03.020

[14] Papastergiou, D., & Lebet, J.P. (2014). Design and Experimental Verification of an Innovative Steel-Concrete Composite Beam， J. CONSTR. STEEL RES., 93, 9-19. http://dx.doi.org/10.1016/j.jcsr.2013.10.017

[15] FHWA. Connection details for prefabricated bridge elements and systems, FHWA-IF-09-010, office of engineering., bridge division, Washington, DC, US, 2009.

[16] Ahmed S., & Karavasilis, T. (2018). Removable shear connector for steel-concrete composite bridges, STEEL COMPOS. STRUCT., 29. 107-123. http://dx.doi.org/10.12989/scs.2018.29.1.107

[17] Su, Q., & Li Y. (2015). Shear capacity of grouped stud connector embedded by high strength mortar, J. TONGJI UNI. (natural science), 43(5):699-705. (in Chinese) http://dx.doi.org/10.11908/j.issn.0253-374x.2015.05.008

[18] Balkos, K.D., Sjaarda, M., West, J.S., & Walbridge, S. (2019). Static and fatigue tests of steel-precast composite beam specimens with through-bolt shear connectors, J. BRIDGE ENG., 24(5): 04019036. http://dx.doi.org/10.1061/(ASCE)BE.1943-5592.0001382.

[19] Chen, Y.T., Zhao, Y., West, J.S., & Walbridge, S. (2014). Behavior of steel–precast composite girders with through-bolt shear connectors under static loading, J. CONSTR. STEEL RES., 103 168–178. http://dx.doi.org/10.1016/j.jcsr.2014.09.001

[20] Liu, X., Bradford, M. A., & Ataei, A. (2017). Flexural performance of innovative sustainable composite steel-concrete beams, ENG. STRUCT., 130:282-296. http://dx.doi.org/10.1016/j.engstruct.2016.10.009

[21] Zhou, Z.X. (2012). Prestressed steel- concrete composite continuous rigid frame bridge and construction: China, ZL 200910104675. X, Patent Office of China. (in Chinese)

[22] Zhou, Z.X. (2014), the Shear Connectors of PCSS: Germany, PCT/CN2014/075541. German Patent Office. (in German)

[23] Gao, Y.M., Zhou, Z.X., Liu, D., & Wang Y. (2016). Cracking of a prefabricated steel truss-concrete composite beam with pre-embedded shear studs under hogging moment, STEEL COMPOS. STRUCT., 5: 981-997. http://dx.doi.org/10.12989/scs.2016.21.5.981

[24] MHURD of China. Code for design of steel and concrete composite bridges (GB 50917-2013), JHPRESS, Beijing, China, 2013. (in Chinese)

[25] MOT of China. Specifications for design of highway reinforced concrete and prestressed concrete bridges and culverts (JTG 3362-2018), CCPRESS, Beijing, China, 2018. (in Chinese)

[26] Oehlers, D.J, & Bradford M. (1999). Elementary Behaviour of Composite Steel and Concrete Structural Members, Butterworth-Heinemann [J], 1999: 21-38.

[27] Chen, Y., Lu, P., Song, X., & Liu, Y. (2012). Test Study of Shear Performance of Shear Studs for Steel-Concrete Composite Beams. Bridge Construction, 42(3): 63-69.

[28] Zhong, Q. (2017). The experimental study on composite steel-prefabricated precast concrete slab beam. Hunan University.

[29] Xue, W., Ding, M., Wang, H., & Luo, Z. (2009). Experimental studies on behavior of stud shear connectors under monotonic loads. 30 (1): 95-100.

[30] Zhang, J., Hu, X., Fu, W., Du, H., Sun, Q., & Zhang, Q. Experimental and theoretical study on longitudinal shear behavior of steel-concrete composite beams, J. CONSTR. STEEL RES.,171:1-18. http://10.1016/j.jcsr.2020.106144

[31] Luo, Y. (2008). Research on shear Connectors of Steel-concrete composite Beams. Central South University.

[32] Oehlers, D.J., & Park, S.M. (1992). Shear Connectors in Composite Beams with Longitudinally Cracked Slabs. J STRUCT. ENG., 118(8):2004-2022. http://118(8):2004-2022.10.1061/(asce)0733-9445(1992)118:8(2004)

[33] Xue, D., Liu, Y., Yu, Z., & He J. (2012). Static behavior of multi-stud shear connectors for steel-concrete composite bridge. J. CONSTR. STEEL RES., 74(8):1-7. http://10.1016/j.jcsr.2011.09.017

[34] Li, M. (2015). Refined Calculation Method and Time-Dependent Behaviors of Stud Connectors in Steel-Concrete Composite Girder Bridges. Southeast University.

[35] Xu, C., Sugiura, K. (2013). FEM analysis on failure development of group studs shear connector under effects of concrete strength and stud dimension. ENG. FAIL. ANAL., 35:343-354. http://10.1016/j.engfailanal.2013.02.023

[36] Dassault Systèmes. Abaqus software Vélizy-Villacoublay, France. https://www.abaqus.com/

[37] Zhao, J., & Nie J. (2009). Nonlinear finite element analysis of steel plate-concrete composite beams, ENG. MECH., 26(4) 105-112.

[38] Faham, T., Gianluca, R., & Lessandro, Z. (2013). Probabilistic three-dimensional finite element study on composite beams with steel trapezoidal decking. J. CONSTR. STEEL. RES., 80:394-411. http://: 10.1016/j.jcsr.2012.10.003

[39] Nie J., & Wang Y. (2013). Comparison study of constitutive model of concrete in ABAQUS for static analysis of structures, ENG. MECH., 30 (4): 59-67. (in Chinese)

[40] Guo, Z., & Shi, X. Principles and analysis of reinforced concrete, Tsinghua University Press, Beijing, China, 2003. (in Chinese)

[41] MHURD of China. Code for design of concrete structures (GB 50010-2010). CABP, Beijing, China, 2010.

[42] Hordijk, D. (1992). Tensile and tensile fatigue behaviour of concrete: experiments, modelling and analyses, Heron 37: 3 - 79.

[43] CEN, Eurocode 3 – Design of steel structures – Part 1-5: Plated structural elements, CEN, Brussels, 2006.

[44] MHURD of China. Technical code for safety appraisal of engineering structural strengthening materials (GB 50728-2011). CABP, Beijing, China, 2011.

[45] Luccioni, B.M., López, D.E., & Danesi, R.F. (2005). Bond-slip in reinforced concrete elements. J. STRUCT. ENG., 131(11), 1690-1698. https://doi.org/10.1061/(ASCE)0733-9445(2005)131:11(1690)

[46] Kankam, C.K. (1997). Relationship of bond stress, steel stress, and slip in reinforced concrete. J. STRUCT. ENG., 123(1), 79-85. https://doi.org/10.1061/(ASCE)0733-9445(1997)123:1(79)